Progress In Electromagnetics Research Letters, Vol. 106, 129–134, 2022

Design of Cylindrical Holographic Impedance Metasurface for Near-Field Focusing

Heng Wang, Shixing Yu, and Na Kou*

Abstract—In this paper, a design method for near-field focusing cylindrical holographic impedance metasurfaces is proposed. Firstly, based on the design theory of planar holographic impedance metasurface, we deduce the design formula for cylindrical holographic impedance metasurface by using the method of major axis matching. Then the feasibility of theoretical analysis is verified by simulation and measurement. The results show that the design method can effectively realize the near-field focusing, which can provide a reference for the application of conformal devices for microwave hyperthermia and energy harvesting.

1. INTRODUCTION

The near-field focusing antenna can focus the electromagnetic wave energy to a specified position in the near-field area of the antenna [1]. The principle is to adjust the phase of each array element on the antenna aperture to realize the in-phase superposition of the energy at a certain point or multiple points, thus achieving the focusing effect in the near-field area [2]. Near-field focusing antennas are widely used in biomedical microwave hyperthermia [3], industrial microwave imaging technology [4], and energy harvesting [5].

At present, there are many methods to realize near-field focusing. The most traditional near-field focusing antenna is the lens-focused antenna based on geometric optics [6]. It is the most direct way to achieve near-field focusing, but it is bulky, and the manufacturing cost and difficulty are high. Fresnel zone plate is an improved method of a dielectric lens antenna that filters out electromagnetic waves of the desired phase through annular metal strips [7]. Compared with the traditional dielectric lens, it has the advantages of simple structure, low cost, low profile, and light weight, but the efficiency is lower than that of the traditional lens, and some unnecessary electromagnetic waves will be reflected. The focusing principle of transmitarray and reflectarray is the same as that of dielectric lens antenna [8, 9]. They both modulate the wavefront phase and focus the energy to the required focus, which can achieve focusing more effectively. However, they all have the defects of large mass, high profile, and high cost. Phased array antenna is considered as an ideal choice to realize near-field focusing because of their very flexible control of energy distribution [10]. However, the feed network of phased array antenna is complex which limits its wide application in practice.

The discovery of metamaterials provides a new way for electromagnetic wave regulation [11]. In particular, two-dimensional metasurface can be used to modulate the phase, amplitude, and polarization of electromagnetic waves [12]. In addition, it has the advantages of light weight, simple structure, and low profile. There are three main types of metasurfaces, reflective metasurfaces [13], transmitted metasurfaces [14], and holographic metasurfaces [15]. Compared with reflective metasurfaces and transmitted metasurfaces, holographic metasurfaces have a lower profile and are easier to integrate.

Received 22 June 2022, Accepted 7 September 2022, Scheduled 16 September 2022

* Corresponding author: Na Kou (nkou@gzu.edu.cn).

The authors are with the Key Laboratory of Micro-Nano-Electronics and Software Technology of Guizhou Province, College of Big Data and Information Engineering, Guizhou University, Guiyang 550025, China.

Holographic metasurface can control the propagation and radiation of metasurface waves by changing the sizes of metasurface units to form effective impedance distribution [16]. However, the above-mentioned near-field focusing antennas are usually in planar form. For medical microwave hyperthermia, the mismatch between the antenna and the shape of the medical device will bring inconveniences. Considering that the feed source is in the same plane as the holographic metasurface, it can be well conformed to the required device to achieve near-field focusing. In this paper, a cylindrical holographic impedance metasurface that can generate near-field focusing is proposed. A monopole feed is integrated with the holographic impedance metasurface on the same surface, and multiple focusing points can be generated. The architecture of the paper is organized as follows. In Section 2, we present the design formula and method of the cylindrical holographic impedance metasurface. In Section 3, we verify the feasibility of the design proposed in Section 2 through simulation and experimental measurements. Section 4 is the conclusion of this paper.

2. FOCUSING PRINCIPLE BASED ON HOLOGRAPHIC THEORY

The structure of the metasurface element designed in this paper is shown in Fig. 1(a). The top layer is a split circular patch, and the bottom layer is ground plane. The radius of the circular patch is r, and the width of the slot is $g_t = 0.1\,\text{mm}$. The angle between direction of the slot and the positive direction of the X-axis is θ_t, and the element period is $P = 3\,\text{mm}$. Furthermore, in order to bend the designed metasurface well, we use a relatively soft Wangling F4b support substrate with thickness h of 0.5 mm, relative permittivity ε_r of 2.65, and loss angle $\tan\delta$ of 0.003.

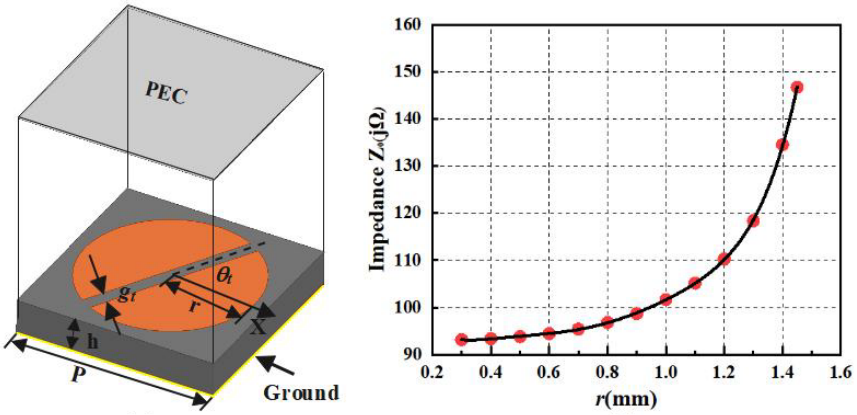

Figure 1. (a) Geometry diagram of the metasurface element. (b) The mapping relationship between the equivalent scalar impedance Z_0 and the radius r of the metasurface element.

We used an eigen-solving method to solve the equivalent scalar impedance of the metasurface element with different r and θ_t. Using the eigenmode solver, the surface wave propagation direction θ_f and the characteristic frequency f can be solved. Next, by selecting three different surface wave propagation directions θ_f, the equivalent scalar impedance Z_0 in different surface wave propagation directions θ_f can be solved by:

$$Z_0 = j\eta_0\sqrt{\left(\frac{\sqrt{\phi_x^2+\phi_y^2}\times c}{2\pi f P}\right)^2 - 1} \tag{1}$$

where ϕ_x and ϕ_y are phase delays along the X-axis and Y-axis, respectively. η_0 is the free space wave impedance, and c is the speed of light. Then, by substituting the equivalent scalar impedance Z_0 corresponding to different θ_f into the following formula, a set of nonlinear equations about tensor

components (Z_{xx}, Z_{xy}, Z_{yy}) can be obtained.

$$Z_0 = j\eta_0\Big\{-j\left(\eta_0^2 + Z_{xx}Z_{yy} - Z_{xy}^2\right) \pm \Big[-\left(\eta_0^2 + Z_{xx}Z_{yy} - Z_{xy}^2\right)^2 + 4\eta_0^2 \times \left(Z_{xx}\sin^2\theta_f + Z_{yy}\cos^2\theta_f - Z_{xy}\sin 2\theta_f\right) \times \left(Z_{xx}\cos^2\theta_f + Z_{yy}\sin^2\theta_f + Z_{xy}\sin 2\theta_f\right)\Big]^{\frac{1}{2}}\Big\} \times \left[2\eta_0\left(Z_{xx}\sin^2\theta_f + Z_{yy}\cos^2\theta_f - Z_{xy}\sin 2\theta_f\right)\right]^{-1} \quad (2)$$

Finally, we solved the nonlinear equations to obtain the effect of different surface wave propagation angles θ_f on the equivalent scalar impedance Z_0, as shown in Fig. 2(a).

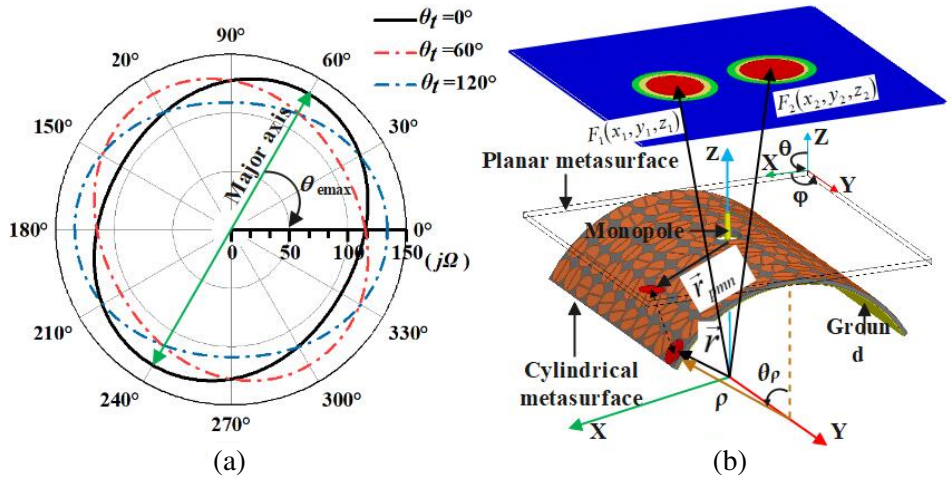

Figure 2. (a) The effect of different surface wave propagation angle θ_f on the equivalent scalar impedance Z_0. (b) Schematic diagram of a metasurface antenna for near-field focusing.

The relationship between the equivalent scalar impedance Z_0 of anisotropic metasurface element and the angle θ_f is elliptical. The value of the major axis is almost unchanged with the change of θ_t, and the angle θ_e max of the major axis is approximately equal to θ_t. Therefore, we ignored the effect of θ_t on the equivalent scalar impedance of the metasurface element and adopted a simple matching method in which the radius r of the metasurface element corresponds to the major axis of the equivalent scalar impedance Z_0. The relationship between the radius r of the metasurface unit and the major axis of the equivalent scalar impedance Z_0 is shown in Fig. 1(b), and their relationship can be expressed as follows:

$$Z_0 = 133 \times r^7 - 480 \times r^6 + 541 \times r^5 + 2 \times r^4 - 443 \times r^3 + 354 \times r^2 - 110 \times r + 105 \quad (3)$$

The schematic diagram of the metasurface antenna to achieve near-field focusing is shown in Fig. 2(b). Based on the holographic theory [17], the tensor impedance of the metasurface at each position can be deduced inversely through the preset radiation wave and the excitation wave on the metasurface antenna. The position distribution of the tensor impedance component (Z_{xx}, Z_{xy}, Z_{yy}) is calculated as follows ($Z_{xy} = Z_{yx}$ according to the reciprocity theorem):

$$Z = j\begin{pmatrix} Z_{xx} & Z_{xy} \\ Z_{yx} & Z_{yy} \end{pmatrix} = j\begin{pmatrix} X_m & 0 \\ 0 & X_m \end{pmatrix} + j\frac{M}{2}\mathrm{Im}\left(E_{pre} \otimes J_{sur}^H - J_{sur} \otimes E_{pre}^H\right) \quad (4)$$

where X_m is the average impedance, and M is the modulation depth. The near-field of metasurface antenna with multiple focal points at different positions can be expressed as follows:

$$E_{pre} = (1, 0, 0)\sum_{i=1}^{i=N} \exp\left(jk_0\left|\vec{F}_i - \vec{r}\right|\right) \quad (5)$$

The metasurface is excited by the monopole antenna, and the surface current on the metasurface can be expressed as:

$$J_{sur} = \frac{(x, y, 0)}{|\vec{r}_{pmn}|} \exp\left(-j\vec{k}_t \cdot \vec{r}_{pmn}\right) \tag{6}$$

Substituting Eqs. (5) and (6) into Eq. (4) yields an expression for the tensor impedance component (Z_{xx}, Z_{xy}, Z_{yy}):

$$\begin{cases} Z_{xx} = j\left[X_m + \frac{M}{|\vec{r}_{pmn}|} x_{pmn} \sum\limits_{i=1}^{i=N} \sin\left(\left|\vec{k}_t\right| \cdot |\vec{r}_{pmn}| + k_0 \left|\vec{F}_i - \vec{r}\right|\right)\right] \\ Z_{xy} = j\frac{M}{2|\vec{r}_{pmn}|}\left(y_{pmn} + x_{pmn}\right) \sum\limits_{i=1}^{i=N} \sin\left(\left|\vec{k}_t\right| \cdot |\vec{r}_{pmn}| + k_0 \left|\vec{F}_i - \vec{r}\right|\right) \\ Z_{yy} = j\left[X_m + \frac{M}{|\vec{r}_{pmn}|} y_{pmn} \sum\limits_{i=1}^{i=N} \sin\left(\left|\vec{k}_t\right| \cdot |\vec{r}_{pmn}| + k_0 \left|\vec{F}_i - \vec{r}\right|\right)\right] \end{cases} \tag{7}$$

where k_0 is the propagation constant in vacuum. The surface wave propagation constant k_t, $\vec{r}_p mn$, and $\vec{r}$ can be expressed as:

$$\begin{cases} \left|\vec{k}_t\right| = \sqrt{k_0 \times \left(1 + \left(X_m/\eta_0\right)^2\right)} \\ \vec{r}_{pmn} = \vec{e}_x x_{pmn} + \vec{e}_y y_{pmn} \\ \vec{r} = \vec{e}_x \rho \sin\theta_\rho + \vec{e}_y y + \vec{e}_z \rho \cos\theta_\rho \end{cases} \tag{8}$$

3. METASURFACE DESIGN AND EXPERIMENTS

In order to verify the near-field focusing performances, we designed and fabricated a metasurface antenna prototype which is capable of generating double focusing points at $f = 24.125$ GHz. The positions of the two focusing points are F_1 (0.03, 0, 0.2 m) and F_2 (−0.03, 0, 0.2 m). The calculated holograms of radius r and angle θ_t in the metasurface element are shown in Fig. 3(a) and Fig. 3(b).

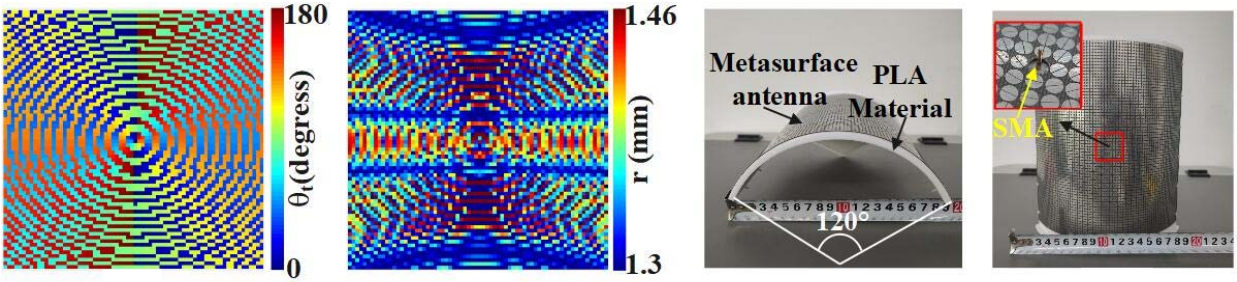

Figure 3. Distributions of (a) r and (b) θ_t for generating near-field focusing by the cylindrical metasurface antenna, (c) side and (d) front faces of the designed cylindrical metasurface antenna.

The fabricated metasurface antenna is composed of 71 × 71 elements with dimension of 213 mm × 213 mm in planar form, and the size of conformal cylindrical form is 176 mm × 213 mm with bending angle of 120°, as shown in Fig. 3(c) and Fig. 3(d). In order to prevent the metasurface units from being oxidized, the surface process adopts tin precipitation operation. We also use the 3-D printing technology and polylactic acid (PLA) material to print the required cylindrical bracket. In order to make the metasurface antenna fit on the cylindrical surface well, location holes are punched at both ends of its bending direction (X-axis direction). Nylon screws are used to connect these holes with the fabricated metasurface. Finally, a SubMiniature Version A (SMA) connector with a probe radius of 0.32 mm was welded to the back of the metasurface antenna. The monopole feed is made by the probe protruded 3.1 mm (quarter wavelengths at operating frequency) from a hole with a radius of 1.5 mm at the center of the metasurface antenna.

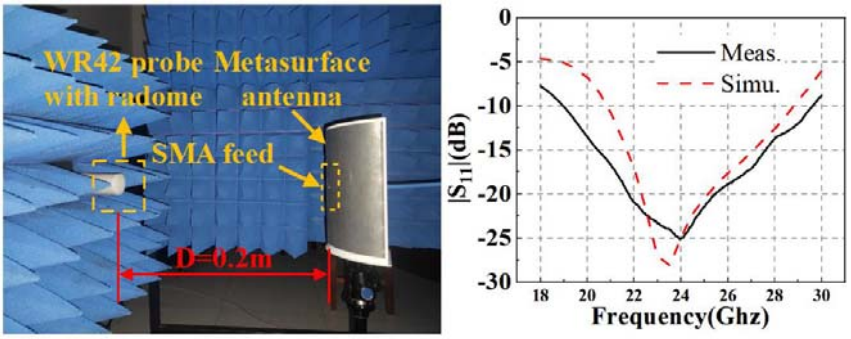

Figure 4. (a) Measurement system configuration. (b) Simulated and measured reflection coefficients of the designed cylindrical metasurface antenna.

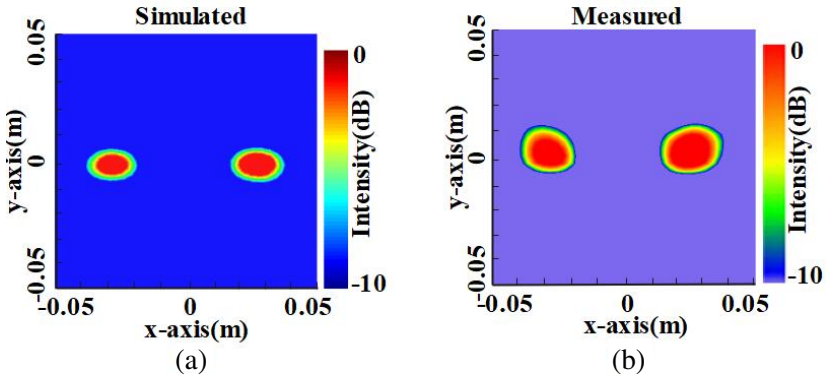

Figure 5. Simulated and measured horizontally polarized E-field distributions at 24.125 GHz.

We measured the horizontal E-field component at the operating frequency $f = 24.125$ GHz by the near-field planar scanning technique, as shown in Fig. 4(a). Fig. 4(b) shows the comparison of the reflection coefficients of the designed metasurface antennas between simulation and measurement. It shows that the two results agree well with each other, and the frequency range where the reflection coefficient is below -15 dB is from 20.5 GHz to 27.5 GHz with the relative bandwidth being 29 %. The horizontally polarized E-field distribution on the scanning plane with size of $0.1 \times 0.1\,\mathrm{m}^2$ (41×41 sampling points) was measured at the distance of 0.2 m from the metasurface antenna, as shown in Fig. 5(b). The simulated E-field distribution is shown in Fig. 5(a) for comparison. We can observe that two focusing points can be clearly recognized at the designed positions. However, the measured focusing area is a little larger than the simulated one. This can be attributed to the following reasons: first, the accuracy of 3-D printing is relatively large, leading to errors in the bending angle. Second, the phase error of the surface wave propagation on the metasurface appears when the SMA's probe is not in the center of the metasurface due to the manual welding process. Finally, there are noise and reflections in the measured environment.

4. CONCLUSION

Holographic metasurface can be regulated according to the feed radiation field to obtain the required radiation field. Compared with the traditional antenna structure, it has the advantages of low profile, simple feeding structure, low cost, easy processing, and is conformal. It is expected to replace the traditional phased array antenna, avoiding complex electronic control network and achieving near-field focusing. In this paper, a cylindrical holographic impedance metasurface that can realize near-field focusing is proposed based on theoretical analysis and formula derivation. Simulation and measurement

both show that the designed metasurface antenna can effectively generate focusing points in the near-field area. In addition, conformal designs can satisfy some non-planar requirements.

ACKNOWLEDGMENT

This work was supported by the National Natural Science Foundation of China under Grant No. 61961006 and the Science and Technology Foundation of Guizhou Province under Grant No. QKHJC[2020]1Y256.

REFERENCES

1. Buffi, A., P. Nepa, and G. Manara, "Design criteria for near-field-focused planar arrays," *IEEE Antennas Propag. Mag.*, Vol. 54, No. 1, 40–50, 2012.
2. Karimkashi, S. and A. A. Kishk, "Focused microstrip array antenna using a Dolph-Chebyshev near-field design," *IEEE Trans. Antennas Propag.*, Vol. 57, No. 12, 3813–3820, 2009.
3. Nguyen, P. T., A. M. Abbosh, and S. Crozier, "3-D focused microwave hyperthermia for breast cancer treatment with experimental validation," *IEEE Trans. Antennas Propag.*, Vol. 62, No. 7, 3489–3500, 2017.
4. Li, P.-F., S.-W. Qu, and S. Yang, "Two-dimensional imaging based on near-field focused array antenna," *IEEE Antennas Wirel. Propag. Lett.*, Vol. 18, No. 2, 274–278, 2018.
5. Li, L., et al., "Progress, challenges, and perspective on metasurfaces for ambient radio frequency energy harvesting," *Appl. Phys. Lett.*, Vol. 116, No. 6, 060501, 2020.
6. Reid, D. R. and G. S. Smith, "A comparison of the focusing properties of a Fresnel zone plate with a doubly-hyperbolic lens for application in a free-space, focused-beam measurement system," *IEEE Trans. Antennas Propag.*, Vol. 57, No. 2, 499–507, 2009.
7. Karimkashi, S. and A. A. Kishk, "Focusing properties of Fresnel zone plate lens antennas in the near-field region," *IEEE Trans. Antennas Propag.*, Vol. 59, No. 5, 1481–1487, 2011.
8. You, B., Y. Liu, J. Zhou, and H. Chou, "Numerical synthesis of dualband reflectarray antenna for optimum near-field radiation," *IEEE Antennas Wirel. Propag. Lett.*, Vol. 11, 760–762, 2012.
9. Plaza, E. G., et al., "An ultrathin 2-bit near-field transmitarray lens," *IEEE Antennas Wirel. Propag. Lett.*, Vol. 16, 1784–1787, 2017.
10. Li, Y., et al., "Cylindrical conformal array antenna for near field focusing," *Int. J. RF Microw. Comput.-Aid. Eng.*, Vol. 32, No. 6, e23135, 2022.
11. He, Q., S. L. Sun, S. Y. Xiao, et al., "Manipulating electromagnetic waves with metamaterials: Concept and microwave realizations," *Chin. Phys. B*, Vol. 23, No. 4, 047808, 2014.
12. Holloway, C. L., E. F. Kuester, and D. Novotny, "Waveguides composed of metafilms/metasurfaces: The two-dimensional equivalent of metamaterials," *IEEE Antennas Wirel. Propag. Lett.*, Vol. 8, 525–529, 2009.
13. Yu, S., et al., "Design of dual-polarized reflectarray for near-field shaped focusing," *IEEE Antennas Wirel. Propag. Lett.*, Vol. 20, No. 5, 803–807, 2021.
14. Huang, H. and J. Zhang, "Multifunctional near field focusing transmission metasurface based on polarization sensitivity," *Microw. Opt. Technol. Lett.*, Vol. 63, No. 7, 1868–1874, 2021.
15. Pandi, S., C. A. Balanis, and C. R. Birtcher, "Design of scalar impedance holographic metasurfaces for antenna beam formation with desired polarization," *IEEE Trans. Antennas Propag.*, Vol. 63, No. 7, 3016–3024, 2015.
16. Fong, B. H., et al., "Scalar and tensor holographic artificial impedance surfaces," *IEEE Trans. Antennas Propag.*, Vol. 58, No. 10, 3212–3221, 2010.
17. Pandi, S., C. A. Balanis, and C. R. Birtcher, "Design of scalar impedance holographic metasurfaces for antenna beam formation with desired polarization," *IEEE Trans. Antennas Propag.*, Vol. 61, No. 4, 1403–1413, 2013.